RESEARCH ARTICLE

A TiO_2-Co(terpyridine)$_2$ photocatalyst for the selective oxidation of biomass to formate coupled to the reduction of CO_2 to syngas

Erwin Lam[a], Erwin Reisner*[a]

[a] Dr. E. Lam, Prof. E. Reisner
Yusuf Hamied Department of Chemistry
University of Cambridge
Lensfield Road, CB2 1EW, Cambridge, UK
E-mail: reisner@ch.cam.ac.uk

Supporting information for this article is given via a link at the end of the document.

Abstract: Immobilization of a phosphonated cobalt bis(terpyridine) catalyst on TiO_2 nanoparticles generates a hybrid photocatalyst that allows coupling aqueous CO_2-to-syngas (CO and H_2) photoreduction to selective oxidation of biomass-derived oxygenates or cellulose to formate. An enzymatic saccharification pre-treatment process is employed that enables the use of insoluble cellulose as a substrate under benign conditions suitable for CO_2 conversion. The photocatalyst consists of solely earth-abundant components, and its heterogeneous nature allows for reuse and operation in aqueous solution for several days at 25 °C, reaching a cellulose-to-formate conversion yield of 17%. Thus, the proof-of-concept for valorizing two waste streams (CO_2 and biomass) simultaneously into value-added chemicals through solar-driven catalysis is demonstrated.

Introduction

Photocatalysis can utilize sunlight to perform various kinds of sustainable chemical transformations.[1-4] One green chemistry approach is the photo-oxidation of solid waste streams such as biomass coupled to the simultaneous reduction of protons for the generation of value-added oxidation products and the energy carrier H_2.[5-8] This photoreforming (PR) process relies typically on a semiconductor particle that absorbs light to generate excited electrons to catalyze the reduction of water to H_2, while holes are being used to oxidize the organic waste.[5, 9] An archetypical semiconductor for PR is TiO_2 coupled with various kinds of H_2 evolving co-catalysts such as Pt, RuO_2, MoS_2 or Ni_2P,[10-14] especially since TiO_2 is a stable, inexpensive and scalable semiconductor suitable for PR of biomass such as glucose.[5, 15-16]

However, PR could in principle also be coupled to alternative photoreduction reactions such as the valorization of the greenhouse gas CO_2 to produce valuable carbon-based energy carriers.[17-19] PR of aqueous CO_2 to CO or syngas (a gas mixture of H_2 and CO that acts as a precursor for industrial bulk chemicals such as methanol and hydrocarbons) is therefore an attractive proposition since their production currently requires fossil fuels.[20-21] There are several potential sources of CO_2 for such a process (*e.g.*, flue gas in industry, fermentation plants or direct air carbon capture technologies) and extending PR to CO_2 valorization could therefore contribute towards the implementation of a circular carbon-neutral economy.[1, 17]

Despite this promise, the coupling of photocatalytic CO_2 reduction with waste valorization has not yet been reported and current CO_2 photoreduction catalysts rely on unsustainable sacrificial electron donors for the oxidation half-reaction or, in few cases, coupling to oxygen evolution from water.[3, 22-24] An additional challenge arises from the conduction band (CB) location of TiO_2,[25-27] providing insufficient driving force for the best available CO_2-to-CO reducing solid state electrocatalysts. Furthermore, the common requirement of extreme pH values to depolymerize cellulose for use in photocatalysis prevents the effective coupling with CO_2 utilization that typically requires operation at near neutral-pH.[28]

Recently, molecular 3d-transition metal complexes with a relatively low overpotential for aqueous CO_2 reduction have emerged as surface-anchored catalysts in electro- and photocatalysis.[28-30] In particular, the combination of a cobalt complex bearing phosphonated terpyridine ligands immobilized on a porous TiO_2 scaffold on a Si photoelectrode enabled the (photo)electroreduction of aqueous CO_2 to CO.[29] Immobilization of the metal complex altered the mechanism for CO_2 reduction, resulting in a catalyst that operates at a small overpotential. This recent finding opens new possibilities to explore solar-driven CO_2 photoreduction systems using molecular components integrated with semiconductors such as TiO_2 with the possibility to couple organic oxidation chemistry in water.

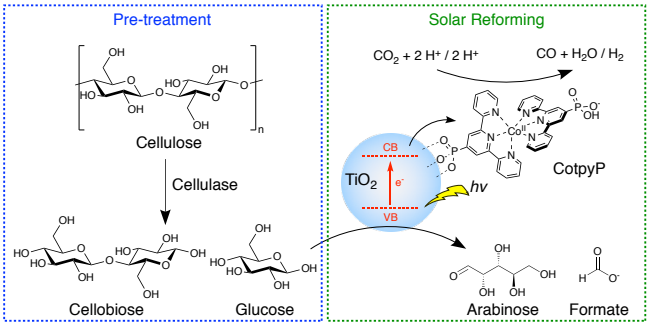

Scheme 1. Schematic representation of enzymatic cellulose pre-treatment to generate soluble organic substrates (cellobiose and glucose), which can subsequently be photo-reformed in aqueous CO_2 to give formate and syngas.

Here, we introduce a closed photocatalytic system that combines photoreduction of CO_2 with photo-oxidation of biomass derived oxygenates and cellulose. We first optimize our photocatalyst for the photoreduction of CO_2 using a sacrificial electron donor and then replace it by soluble biomass-derived monomers. Finally, we access insoluble polymeric biomass substrates for photocatalysis

by replacing the usually harsh pre-treatment condition not suitable for molecular CO_2 reduction catalysis by an enzymatic procedure that allows to breakdown polymeric biomass substrates under benign conditions (Scheme 1).

Results and Discussion

A molecular cobalt(II) catalyst bearing two 4'-phosphonated 2,2':6',2''-terpyridine ligands with BF_4^- as counter anions (denoted as **CotpyP**) was synthesized and characterized according to a previous procedure.[29] The phosphonate moiety acts as an anchoring group for immobilization on metal oxides, including TiO_2 (Scheme 1).[31] We first investigated the interaction of **CotpyP** with TiO_2 (P25, anatase-rutile, particle diameter ~20 nm, 50 $m^2\ g^{-1}$) and the maximum loading capacity for **CotpyP** on TiO_2. An excess **CotpyP** (150 nmol) was stirred in a suspension of TiO_2 (2.5 mg) in a MeCN:H_2O (2:1 v:v; 1.5 mL) mixture for 3 h at room temperature. The TiO_2|**CotpyP** hybrid material was then separated by centrifugation, washed with MeOH and dried under vacuum (10^{-2} mbar) at room temperature. Quantifying the remaining **CotpyP** in the supernatant of the incubation solution by UV/Vis spectrophotometry showed the immobilization of 41±1 μmol **CotpyP** $g_{TiO_2}^{-1}$ (0.49 ± 0.01 Co nm^{-2} based on the specific surface area of TiO_2 (50 $m^2\ g^{-1}$); Figures S1-S2). A similar cobalt content of 39 μmol **CotpyP** $g_{TiO_2}^{-1}$ was also determined by inductively coupled plasma optical emission spectrometry of the isolated solid TiO_2|**CotpyP** dissolved in H_2SO_4.

Attachment of the molecular **CotpyP** catalyst on TiO_2 was also confirmed by several solid-state techniques. Fourier-transform infrared (FT-IR) spectroscopy of the TiO_2|**CotpyP** powder shows the presence of new vibrational bands at 1389, 1474, 1587 and 1570 cm^{-1}, which can be assigned to the aromatic rings of **CotpyP** from the molecular complex on TiO_2 (Figure S3).[29] Cobalt was also identified by high-angular annular dark-field imaging and energy dispersive X-ray analysis (Figure S4). Diffuse reflectance UV/Vis spectroscopy of the solid sample revealed new bands appearing at approximately 450 and 500 nm (Figure S3), which can be assigned to metal-to-ligand transitions in **CotpyP**.[32]

The TiO_2|**CotpyP** hybrid was then investigated for CO_2 photoreduction with triethanolamine (TEOA) as a sacrificial electron donor. Photocatalysis was performed in a sealed glass reactor irradiated with simulated solar light (100 mW cm^{-2}, AM 1.5G) in a 3 mL solution of MeCN:H_2O (2:1 v:v) containing TEOA (0.1 M) with a headspace of 4.74 mL. The solution that was purged with CO_2 containing 2% CH_4 as internal gas chromatography standard contained TiO_2 (5 mg) and **CotpyP** (20 μmol $g_{TiO_2}^{-1}$), which self-assembled *in situ* upon stirring for 30 min to give a TiO_2|**CotpyP** photocatalyst suspension. The amount of **CotpyP** per mass TiO_2 is consistent to previously used molecular catalyst loadings and lower than full monolayer coverage to allow for interactions of the TiO_2 surface with organic electron donors.[33] The gaseous products (H_2 and CO) were monitored by periodically analyzing the headspace using gas chromatography and potential solution-phase products such as formate were detected by ion chromatography.

Irradiation produced 1.3±0.1 mmol CO $g_{TiO_2}^{-1}$ (Figure 1a) and 0.87±0.03 mmol H_2 $g_{TiO_2}^{-1}$ (Figure 1b) after 6 h, and 4.7±0.4 mmol CO $g_{TiO_2}^{-1}$ and 2.4±0.1 mmol H_2 $g_{TiO_2}^{-1}$ after 24 h (Figure 1a; Table 1, entry 1). This activity corresponds to a **CotpyP**-based turnover frequency for CO production (TOF_{CO}) of 9.8 ± 0.9 h^{-1}, a turnover number for CO (TON_{CO}) of 236 ± 21 and product selectivities of (64±2)% for CO, (33±2)% for H_2 and (3±2)% for formate after 24 h photocatalysis (Figure S5). An external quantum efficiency (EQE) for CO formation of (1.2±0.1)% was determined using monochromatic light irradiation, with λ = 360 nm and an intensity of ~6 mW cm^{-2} (see Supporting Information and Table S1 for details).

Isotopic labelling experiments with $^{13}CO_2$ and gas phase product analysis by transmission IR spectroscopy following photocatalysis showed solely ^{13}CO as a product, confirming that CO originates from CO_2 (Figure S6). Control experiments in the absence of **CotpyP**, TiO_2, CO_2, TEOA or light showed no or only minor amounts of products from CO_2 reduction (Table 1, entries 2-6 and Table S2).

Table 1. Photocatalytic syngas (CO and H_2) formation after 24 h of simulated solar light irradiation (100 mW cm^{-2}, AM 1.5G) at 25 °C with TEOA (0.1 M) in MeCN:H_2O (3 mL, 2:1 v:v) containing **CotpyP** (100 nmol) and TiO_2 (P25; 5 mg) purged with CO_2, including exclusion control experiments.

Entry	Removed component	CO [mmol $g_{TiO_2}^{-1}$]	H_2 [mmol $g_{TiO_2}^{-1}$]
1	None	4.7±0.4	2.4±0.1
2	No **CotpyP**	0.03±0.01	0.22±0.01
3	No TiO_2	<0.01	<0.01
4	No CO_2 (N_2 atmosphere)	<0.01	4.4±0.3
5	No TEOA	<0.01	<0.01
6	No Light	<0.01	<0.01

CotpyP has previously already been immobilized on a porous TiO_2 scaffold integrated with a silicon photocathode,[29] but TiO_2 was not photoexcited and only acted as an anchoring site and electron conduit for the immobilized **CotpyP**.[29] In contrast, the TiO_2|**CotpyP** system presented in this study operates by direct photoexcitation of TiO_2, followed by transfer of conduction band electrons to **CotpyP** to form a reduced Co(I) species,[29, 34] while the generated electron hole on TiO_2 is regenerated by TEOA as the sacrificial electron donor, which forms a N-centered radical followed by further oxidation.[35] CO_2 then binds to the reduced **CotpyP** catalyst (after opening of a vacant site presumably by detachment of a pyridine moiety from the Co center)[29] and is then reduced to CO. Therefore, direct photoexcitation of TiO_2 is essential and it allows investigation of the photogenerated holes on TiO_2 to oxidize biomass through radical formation (see below).[5] The presence of MeCN in H_2O is known to shift the conduction band potential of TiO_2 more negative due to a change in the proton adsorption-desorption equilibrium,[36] which facilitates the turnover of the cobalt catalyst.[37] Nevertheless, we note that MeCN is not strictly required as CO production with TiO_2|**CotpyP** is also observed in purely aqueous solution but at approximately four times lower activity (1.09±0.10 mmol CO

$g_{TiO_2}^{-1}$) compared to a MeCN:H_2O mixture (Figure S7 and Table S3). TiO_2|**CotpyP** represents therefore the first precious-metal free metal complex-TiO_2 hybrid material for CO_2 photoreduction.[33, 37-39] Previous molecular catalyst-TiO_2 hybrid materials required rhenium- or ruthenium-based synthetic catalysts,[33, 37-40] or enzymes such as carbon monoxide dehydrogenase and formate dehydrogenase.[41-42]

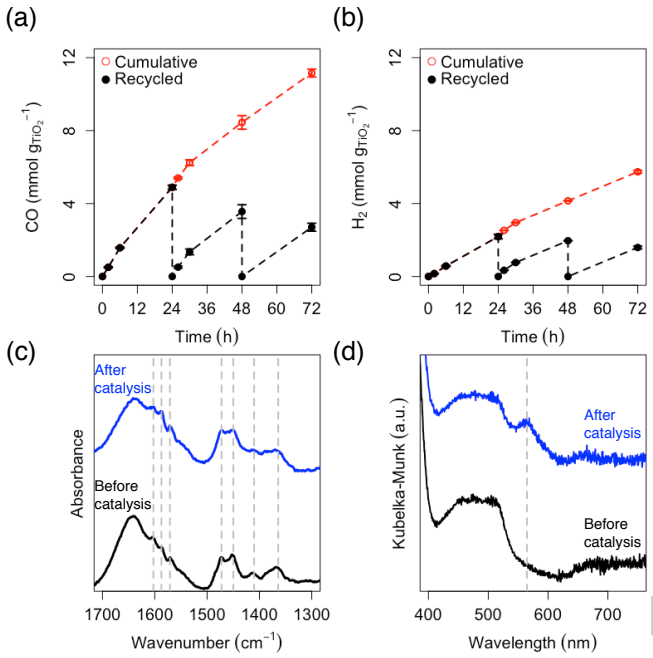

Figure 1. Photocatalytic (a) CO and (b) H_2 formation using TiO_2|**CotpyP** in a CO_2-saturated TEOA/MeCN:H_2O solution. The photocatalyst was recycled after 24 h by removing the supernatant and addition of a fresh TEOA/MeCN:H_2O solution purged with CO_2. The black solid circles show the products formed for each cycle and the red hollow circles the accumulated products. (c) FT-IR and (d) diffuse reflectance UV/Vis spectra of TiO_2|**CotpyP** generated in a CO_2 purged TEOA/MeCN:H_2O solution before (black traces) and after 24 h irradiation (blue traces). Conditions for photocatalysis: simulated solar light (100 mW cm^{-2}, AM 1.5G) in 3 mL of CO_2-purged MeCN:H_2O (2:1 v:v) containing TEOA (0.1 M), TiO_2 (P25; 5 mg) and **CotpyP** (20 μmol $g_{TiO_2}^{-1}$) at 25 °C.

The TiO_2|**CotpyP** photocatalyst powder can be recovered by centrifugation and reused by re-suspending in a fresh MeCN:H_2O solution with TEOA, followed by purging with CO_2 and photocatalysis under simulated solar light. The recycled photocatalyst maintains over 70% of its CO_2 reduction activity compared to the previous 24 h irradiation interval (Figure 1a and Table S4; see Supporting Information for details). The slight decrease in photocatalytic activity after recycling is most likely due to minor decomposition of the immobilized **CotpyP** catalyst. The high activity of the recycled photocatalyst supports the stable anchoring of **CotpyP** on TiO_2, which is further corroborated by post-photocatalysis analysis of the hybrid material following centrifugation, washing (MeOH) and drying under vacuum (see Supporting Information for details). The solid photocatalyst shows no significant changes in the IR absorption bands (Figure 1c) and in the crystalline phases by powder X-ray diffraction for the photocatalyst before and after irradiation (Figure S8). The diffuse reflectance UV/Vis spectrum of the solid after catalysis suggests the emergence of a reduced cobalt species at approximately 565 nm (Figure 1d).[34]

Further photocatalysis optimization (24 h irradiation) shows that reducing the **CotpyP** loading to 10 μmol_{Co} $g_{TiO_2}^{-1}$ results in similar activity for CO production (4.9±0.2 mmol $g_{TiO_2}^{-1}$; TON_{CO} of 490±20 (Figures S9 and S10)) and a CO selectivity of (65±2)% (Figure S5), but a further drop in **CotpyP** loading to 2 μmol_{Co} $g_{TiO_2}^{-1}$ decreases the amount of CO formed to 1.86±0.08 mmol $g_{TiO_2}^{-1}$ (TON_{CO} of 930±40; Table S5 and Figure S10) with a CO selectivity of (83±1)% (Figure S5). Lowering the amount of TiO_2 or the TEOA concentration by 50% leads to a drop in CO formation (3.64±0.24 and 3.34±0.32 mmol $g_{TiO_2}^{-1}$, respectively; Figure S9 and Table S5). A reduction in light intensity also decreases activity (0.38±0.04 mmol CO $g_{TiO_2}^{-1}$ under 50 mW cm^{-2} and 0.056±0.004 mmol CO $g_{TiO_2}^{-1}$ under 20 mW cm^{-2} irradiation after 6 h, Figure S11 and Table S6), which indicates that light absorption and charge transfer kinetics contribute to activity limitations of the photocatalyst system. Replacing the anatase:rutile P25 with pure crystalline phases of TiO_2 has an adverse effect on CO formation (2.3±0.4 mmol CO $g_{TiO_2}^{-1}$ using anatase and 0.04±0.01 mmol CO $g_{TiO_2}^{-1}$ using rutile; Figure S12 and Table S7). Mixed phase P25 displays higher activity than pure anatase or rutile, since P25 helps to accumulate charge and reduces charge recombination compared to pure anatase.[43-44] The significantly reduced activity of rutile is most likely due to its more positive conduction band potential, which is unlikely to provide sufficient driving force for **CotpyP**.[44]

After establishing photocatalytic CO_2 reduction with TiO_2|**CotpyP**, we aimed to replace TEOA as a costly sacrificial electron donor that is used in excess by waste-derived hole scavengers to demonstrate value-added oxidation reactions in meaningful conversion yields. Biomass-derived oxygenates[45-46] such as various C_6 (glucose, galactose) and C_5 (arabinose) sugars, disaccharides (maltose) as well as glycerol represent attractive soluble model compounds for this purpose.[47] Photocatalytic experiments were performed under the optimized conditions identified for TEOA, namely *in situ* assembled TiO_2|**CotpyP** with TiO_2 (5 mg) and **CotpyP** (10 μmol $g_{TiO_2}^{-1}$) in a CO_2-purged MeCN:H_2O solution (2:1 v:v; 3 mL) in the presence of a biomass substrate (0.1 M; except for 0.05 M in the case of maltose as it consists of two glucose monomers) irradiated with simulated solar light for 24 h (100 mW cm^{-2}, AM 1.5G).

All oxygenates studied were identified as suitable substrates to source electrons for the photoreduction of aqueous CO_2 (Figures 2a and S13 and Table S8). In the case of glucose, 0.75±0.01 mmol CO $g_{TiO_2}^{-1}$ and 0.53±0.02 mmol H_2 $g_{TiO_2}^{-1}$ are produced. Formate (1.72±0.06 mmol $g_{TiO_2}^{-1}$) and arabinose (1.30±0.01 mmol $g_{TiO_2}^{-1}$) (both quantified by high performance liquid chromatography) are formed as oxidation products (see below). Similar amounts of reduction products were formed with galactose, an alternative C_6-sugar, forming 0.59±0.02 mmol CO $g_{TiO_2}^{-1}$ and 0.58±0.03 mmol H_2 $g_{TiO_2}^{-1}$ along with 1.46±0.08 mmol formate $g_{TiO_2}^{-1}$. For the C_5 sugar arabinose, slightly lower amounts of CO and formate compared to C_6-sugars were formed (0.43±0.04 mmol CO $g_{TiO_2}^{-1}$, 0.74±0.12 mmol H_2 $g_{TiO_2}^{-1}$ and 1.49±0.03 mmol formate $g_{TiO_2}^{-1}$). In contrast, the disaccharide maltose showed a slightly increased amount of CO product formation (0.91±0.04 mmol CO $g_{TiO_2}^{-1}$, 0.72±0.02 mmol H_2 $g_{TiO_2}^{-1}$ and 1.02±0.06 mmol formate $g_{TiO_2}^{-1}$). Glycerol produced the highest amount of reduction products from the biomass-derived oxygenates, with 1.36±0.06 mmol CO $g_{TiO_2}^{-1}$ and 0.72±0.04 mmol

H_2 $g_{TiO_2}^{-1}$ along with 1.00±0.06 mmol formate $g_{TiO_2}^{-1}$. These results show the versatility of TiO_2|**CotpyP** to extract electrons from a wide range of soluble biomass-derived oxygenates for CO_2 valorization.

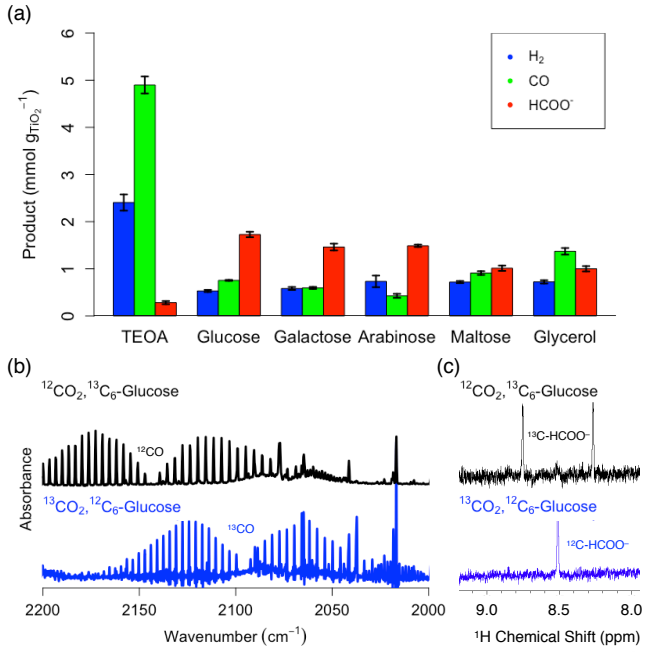

Figure 2. (a) Photocatalytic H_2, CO and formate production with TiO_2|**CotpyP** using different biomass-derived oxygenates as substrates in a CO_2-purged MeCN:H_2O solution. (b) Transmission IR spectra of the headspace gas, (c) ^{1}H NMR spectra in D_2O of the irradiated CO_2-saturated solution with TiO_2|**CotpyP** and glucose using $^{12}CO_2$ and glucose-$^{13}C_6$ (top) showing the production of ^{12}CO and ^{13}C-formate ($J_{C\text{-}H}$ = 195 Hz), and $^{13}CO_2$ and glucose-$^{12}C_6$ (bottom) showing the production of ^{13}CO and ^{12}C-formate (see Supporting Information for details). Conditions for (a-c): 24 h of simulated solar light irradiation (100 mW cm^{-2}, AM 1.5G), 3 mL CO_2-purged MeCN:H_2O (2:1 v:v) containing TiO_2 (P25; 5 mg) and **CotpyP** (10 µmol $g_{TiO_2}^{-1}$) with biomass substrate concentration of 0.1 M for TEOA, glucose, galactose, arabinose and glycerol, and 0.05 M for maltose, 25 °C.

The use of biomass-derived substrates generates a substantially higher amount of formate (>1 mmol $g_{TiO_2}^{-1}$ in all cases; Figure 2a) compared to TEOA (0.28±0.03 mmol $g_{TiO_2}^{-1}$). The high amount of formate accumulated in the solution suggests its production from the oxidative half-reaction *via* PR, and we therefore investigated its source in more detail. Isotopic labelling experiments using $^{13}CO_2$ confirmed that the CO originates from CO_2 by gas phase analysis using transmission IR spectroscopy with glucose as an electron donor (Figure 2b), whereas using $^{13}C_6$-labelled glucose shows that formate originates primarily from the oxidation of glucose by ^{1}H nuclear magnetic resonance (NMR) spectroscopy by the presence of $H^{13}COO^-$ (Figure 2c). An overall glucose-to-formate conversion yield (Scheme S1) of (2.9±0.1)% for the standard photocatalytic conditions was obtained (note that higher yields can be obtained by lowering the initial glucose concentration or increasing the irradiation time, see below).

The reduction of protons to H_2 and CO_2 to CO and the oxidation of glucose to formate (giving arabinose as byproduct, see below) are two-electron processes with an expected 1:1:1 stoichiometric ratio for (H_2+CO):$HCOO^-$:arabinose (Scheme S1). Indeed, a (H_2+CO):$HCOO^-$:arabinose ratio of ~1:1.3:1 is observed for PR of glucose in aqueous CO_2, which supports an excellent selectivity for the photocatalytic reaction (Table S8). The excellent (CO+H_2):$HCOO^-$ stoichiometry is generally found for C_5 and C_6 sugars (glucose, galactose and arabinose) and over a wide range of reaction conditions (solvent mixture and pH) (Table S8-S9). The accumulation of arabinose instead of further oxidation during glucose PR can be explained by its relatively low concentration compared to glucose and slightly lower PR activity compared to glucose (Figure 2a). It is likely that after converting glucose more completely to arabinose, further oxidation of arabinose to different oxidation products would take place. Other possible oxidation products such as gluconic acid or glucaric acid were not detected (Figure S14-S16). The small deviation from the ideal stoichiometry may be due to partially dissolved gas in the solvent mixture (not taken into account in the product analysis), minor amounts of formate originating from CO_2 reduction and minor overoxidation of glucose (*i.e.*, oxidation of some arabinose).[29]

The TiO_2|**CotpyP** photocatalyst (5 mg TiO_2, 10 µmol **CotpyP** $g_{TiO_2}^{-1}$) was characterized after 24 h irradiation in 3 mL of CO_2-saturated TEOA/MeCN:H_2O solution using glucose as the electron donor (see Supporting Information for details). UV/Vis and IR spectra of the solid were recorded before and after photocatalysis and work-up as described above. Comparing the UV/Vis spectra of the hybrid photocatalyst showed that bands from the cobalt complex at approximately 450 and 500 nm were still present after photocatalysis (Figure S17), and additional bands around 430 and 565 nm also appeared, which can be assigned to reduced cobalt species.[34] FT-IR spectra of the solid showed that the vibrational bands corresponding to the terpyridine ligands of **CotpyP** (1571, 1587, 1602 cm^{-1})[29] were still present after photocatalysis, but with a seemingly lower intensity (Figure S17). The changes in the vibrational spectra when using TEOA compared to glucose may be explained by glucose interacting more strongly with the TiO_2 surface and more readily disturbing the interaction between **CotpyP** and TiO_2.[48]

EQEs of (0.30±0.06)% for CO and (1.2±0.1)% for formate were obtained using glucose in CO_2-purged aqueous solution (λ = 360, I = ~6 mW cm^{-2}; see Table S1). Photoreduction of CO_2 coupled to glucose oxidation with TiO_2|**CotpyP** also proceeded in purely aqueous solution, although at a lower activity, producing 0.13±0.01 mmol CO $g_{TiO_2}^{-1}$ and 0.35±0.04 mmol H_2 $g_{TiO_2}^{-1}$ as well as 0.62±0.12 mmol formate $g_{TiO_2}^{-1}$ and 0.27±0.03 mmol arabinose $g_{TiO_2}^{-1}$ after 24 h irradiation (Figure S18 and Table S9).

We next set out to establish the possibility to use polymeric biomass substrates such as cellulose for PR with TiO_2|**CotpyP** in aqueous CO_2. The structural robustness of insoluble cellulose requires the implementation of a suitable pre-treatment procedure to depolymerize cellulose into smaller soluble fragments accessible to the photocatalysts for PR with suitable reaction kinetics.[9] Common procedures in PR include a pre-treatment under strongly alkaline or acidic conditions to hydrolyze cellulose,[9, 49] but these extreme pH conditions are not compatible with the benign conditions required for molecular CO_2 reduction catalysis.[28] We therefore investigated a pretreatment step for cellulose using enzymes such as cellulases to break cellulose down into soluble fragments under near neutral pH conditions.[50-51]

PR of cellulose was therefore performed in a two-step procedure. Cellulose was first enzymatically hydrolyzed into water-soluble fragments (glucose and cellobiose) using cellulase in the dark, which is followed by photocatalytic conversion with TiO_2|**CotpyP** (Scheme 1 and S2). The pre-treatment step is performed by incubating cellulose (40 mg mL^{-1}) with cellulase from *Trichoderma reesei* (2 mg mL^{-1}) in an aqueous solution at pH 5 (50 mM sodium acetate) for 24 h at 37 °C. The suspension was subsequently filtered through a syringe filter (0.2 μm) to obtain a clear solution containing the water-soluble sugars and remaining enzyme. High performance liquid chromatography analysis of the resulting solution shows the generation of glucose (53±2 mM) and cellobiose (26±1 mM), which corresponds to a cellulose-to-glucose/cellobiose yield of (42±2)%.

The pre-treated solution (1 mL) was subsequently diluted with MeCN (2 mL) and used for photocatalysis with the *in situ* assembled TiO_2|**CotpyP** (5 mg TiO_2, 10 $\mu mol_{\mathbf{CotpyP}}$ $g_{TiO_2}^{-1}$). The suspension (3 mL) was then purged with CO_2 and exposed to AM 1.5G irradiation (100 mW cm^{-2}). After 24 h, 0.38±0.02 mmol CO $g_{TiO_2}^{-1}$ (TON_{CO} of 38±2) and 0.38±0.02 mmol H_2 $g_{TiO_2}^{-1}$ as reduction products along with 0.94±0.06 mmol formate $g_{TiO_2}^{-1}$ and 0.28±0.01 mmol arabinose $g_{TiO_2}^{-1}$ as oxidation products were formed (Table 2, entry 1). The ratio between syngas (CO and H_2) and formate was ~0.8, but we observed ~3 times more formate than arabinose (Table S10) because both glucose and cellobiose are present in solution as electron donors that can both produce formate (Figure 2a).

Recyclability was also achieved with TiO_2|**CotpyP** using the pre-treated cellulose solution. Separating the photocatalyst after 24 h irradiation as described above and re-dispersing the solid in a fresh pre-treated cellulose solution (1 mL) diluted with MeCN (2 mL) purged with CO_2 showed that ~55% of the photocatalytic activity with respect to the first cycle is maintained (0.19±0.01 mmol CO $g_{TiO_2}^{-1}$, 0.26±0.01 mmol H_2 $g_{TiO_2}^{-1}$, 0.46±0.06 mmol formate $g_{TiO_2}^{-1}$ and 0.27±0.01 mmol arabinose $g_{TiO_2}^{-1}$ after 24 h irradiation; Figure S19). Another cycle of separating TiO_2|**CotpyP** and reuse resulted in maintaining ~70% of the photocatalytic activity with respect to the previous cycle (0.12±0.02 mmol CO $g_{TiO_2}^{-1}$, 0.18±0.02 mmol H_2 $g_{TiO_2}^{-1}$, 0.39±0.03 mmol formate $g_{TiO_2}^{-1}$ and 0.16±0.02 mmol arabinose $g_{TiO_2}^{-1}$ (Figure S19). Despite a decrease in activity in each recycling step, the photocatalyst can be reused several times in the presence of pre-treated cellulose solution.

We also aimed at increasing the product yields by using a longer irradiation time of a diluted pre-treated cellulose solution. The pre-treated cellulose solution (0.2 mL) was diluted with an aqueous 50 mM sodium acetate (0.8 mL) solution at pH 5, and MeCN (2 mL) was added to give a total volume of 3 mL, which was purged with CO_2. Photocatalysis was performed with the *in situ* assembled TiO_2|**CotpyP** (5 mg TiO_2, 10 $\mu mol_{\mathbf{CotpyP}}$ $g_{TiO_2}^{-1}$) and irradiation with simulated solar light for 72 h (Table 2, entry 2) to produce 0.59±0.02 mmol CO $g_{TiO_2}^{-1}$, 0.97±0.11 mmol H_2 $g_{TiO_2}^{-1}$, 1.64±0.02 mmol formate $g_{TiO_2}^{-1}$ and 0.29±0.01 mmol arabinose $g_{TiO_2}^{-1}$ (Figure S20 and Table S11). Assuming that each monomer unit of sugar forms one equivalent of formate with a 7.0±0.3 mM sugar monomer concentration (3.53±0.13 mM glucose and 1.73±0.07 mM cellobiose), results in a sugar-to-formate conversion yield of (39±2)%. An overall cellulose-to-formate yield was estimated taking into account the cellulose-to-glucose/cellobiose yield of (42±2)% from the pre-treatment step, resulting in an experimental cellulose-to-formate yield of (17±1)%.

Table 2. PR with TiO_2|**CotpyP** of biomass in aqueous CO_2.[a]

Entry	Biomass Source	Irradiation time [h]	CO [mmol $g_{TiO_2}^{-1}$]	H_2 [mmol $g_{TiO_2}^{-1}$]	$HCOO^-$ [mmol $g_{TiO_2}^{-1}$]	Ratio of ($CO+H_2$) to $HCOO^-$	Conversion yield [%][b]
1	Pre-treated Cellulose[c] (34.9±1.3 mM)[d]	24	0.38±0.02	0.38±0.02	0.94±0.06	0.81±0.06	4.5±0.3 (1.9±0.2)
2	Pre-treated Cellulose[c] (7.0±0.3 mM)[d]	72	0.59±0.02	0.97±0.11	1.64±0.02	0.96±0.07	39±2 (17±1)
3	Glucose (100 mM)	24	0.87±0.03	0.60±0.01	1.53±0.05	0.96±0.04	2.6±0.1
4	Glucose (10 mM)	24	0.43±0.04	0.43±0.03	1.18±0.06	0.74±0.06	20±1
5	Cellobiose (10 mM)	24	0.92±0.06	0.72±0.05	1.03±0.08	-	8.6±0.7
6	Cellulose (50 mg w/o pre-treatment)	24	0.046±0.004	0.066±0.018	0.08±0.04	-	(0.13±0.06)[e]
7	Cellulose (5 mg w/o pre-treatment)	24	0.014±0.006	0.048±0.010	0.04±0.02	-	(0.65±0.30)[e]
8	Cellulose pre-treatment condition w/o cellulase	24	<0.01	<0.01	<0.01	-	-
9	Cellulose pre-treatment condition w/o cellulose	24	0.038±0.002	0.05±0.01	0.04±0.01	-	-

[a] Conditions: Solvent mixture of aqueous sodium acetate (1 mL, 50 mM, pH 5) and MeCN (2 mL) purged with CO_2, TiO_2 (P25, 5 mg) and **CotpyP** (10 μmol $g_{TiO_2}^{-1}$), irradiation with simulated solar light (100 mW cm^{-2}, AM 1.5G) for 24 h at 25 °C. [b] Conversion yield was calculated assuming that each soluble monomer unit of sugar ([glucose] + 2 × [cellobiose]) forms one equivalent of formate. Given in brackets are the overall cellulose-to-formate conversion yield based on converting one glucose unit to formate and a cellulose-to-glucose/cellobiose yield of (42±2)% from pre-treatment with cellulase. [c] For pre-treatment procedure see Supporting Information. [d] The donor concentration based on soluble sugar monomer units is given ([glucose] + 2 × [cellobiose]). [e] Cellulose-to-formate conversion yield based on converting one glucose unit to formate.

Photocatalysis under the same experimental condition but using glucose or cellobiose instead of a pre-treated cellulose solution were also performed (Table 2, entries 3-5). For a glucose concentration of 100 mM, 0.87±0.03 mmol CO $g_{TiO_2}^{-1}$ and 0.60±0.01 mmol H_2 $g_{TiO_2}^{-1}$ along with 1.53±0.05 mmol formate $g_{TiO_2}^{-1}$ and 0.91±0.01 mmol arabinose $g_{TiO_2}^{-1}$ were formed after 24 h of photocatalysis. Lowering the glucose concentration to 10 mM slightly decreased the amount of products (0.43±0.04 mmol CO $g_{TiO_2}^{-1}$, 0.43±0.03 mmol H_2 $g_{TiO_2}^{-1}$; 1.18±0.06 mmol formate $g_{TiO_2}^{-1}$, 0.44±0.06 mmol arabinose $g_{TiO_2}^{-1}$), resulting in a glucose-to-formate yield of (20±1)%. For 10 mM cellobiose as electron donor, 0.92±0.06 mmol CO $g_{TiO_2}^{-1}$ and 0.72±0.05 mmol H_2 $g_{TiO_2}^{-1}$ with 1.03±0.08 mmol formate $g_{TiO_2}^{-1}$ were generated. PR using pre-treated cellulose solutions therefore only show slightly lower activities than directly using soluble sugar monomers or dimers (Table 2).

Control experiments without pre-treatment (starting directly from cellulose) or using a pre-treatment solution that was missing either the enzyme or cellulose showed substantially lower activities (< 10%; Table 2, entries 6-9). Thus, the pre-treatment protocol employed in our study is suitable to source electrons for CO_2 photoreduction from polymeric substrates such as cellulose and enables polymeric biomass valorization to produce formate.

Conclusion

A hybrid photocatalyst consisting of a molecular cobalt-terpyridine catalyst anchored on TiO_2 semiconductor nanoparticles is presented. This hybrid system allows for the first demonstration of direct photoexcitation of TiO_2 to generate enough driving force for the reduction of aqueous CO_2 with an integrated 3d transition metal cocatalyst. The CO_2 reduction catalysis at the cobalt complex is subsequently combined with the photo-oxidation of soluble biomass-derived oxygenates and polymeric cellulose on TiO_2. The sunlight-driven conversion of insoluble cellulose was made possible by implementing a two-step protocol that first solubilizes the polymeric biomass through enzymatic saccharification, followed by photoreforming with our hybrid photocatalyst. The enzymatic pre-treatment enables operation at near neutral pH values, which is vital for CO_2 reduction to proceed. The simultaneous photoreforming of CO_2 and polymeric biomass waste streams is unprecedented and does generate two value added products (syngas and formate) with high selectivity. Thus, this work demonstrates the possibility to convert two waste streams in the separate half-reactions of a single photocatalyst to produce sustainable chemical and energy carriers.

Acknowledgements

E.L. acknowledges funding from the Swiss National Science Foundation (Early.Postdoc Fellowship: P2EZP2_191791). Dr. Heather Greer is acknowledged for assistance with electron microscopy (EPSRC; EP/P030467/1). Subhajit Bhattacharjee, Ava Lage, Dr. Stuart Linley, Dr. Christian Pichler and Dr. Santiago Rodríguez-Jiménez (University of Cambridge) are acknowledged for helpful discussions.

Keywords: Photocatalysis • Carbon dioxide fixation • Biomass • TiO_2 • Hybrid Materials

[1] A. M. Appel, J. E. Bercaw, A. B. Bocarsly, H. Dobbek, D. L. DuBois, M. Dupuis, J. G. Ferry, E. Fujita, R. Hille, P. J. A. Kenis, C. A. Kerfeld, R. H. Morris, C. H. F. Peden, A. R. Portis, S. W. Ragsdale, T. B. Rauchfuss, J. N. H. Reek, L. C. Seefeldt, R. K. Thauer, G. L. Waldrop, *Chem. Rev.* **2013**, *113*, 6621.

[2] J. Schneider, M. Matsuoka, M. Takeuchi, J. Zhang, Y. Horiuchi, M. Anpo, D. W. Bahnemann, *Chem. Rev.* **2014**, *114*, 9919.

[3] Q. Wang, K. Domen, *Chem. Rev.* **2020**, *120*, 919.

[4] X. Yang, D. Wang, *ACS Appl. Energy Mater.* **2018**, *1*, 6657.

[5] A. V. Puga, *Coord. Chem. Rev.* **2016**, *315*, 1.

[6] I. Dincer, C. Acar, *Int. J. Hydrogen Energy* **2015**, *40*, 11094.

[7] X. Wu, N. Luo, S. Xie, H. Zhang, Q. Zhang, F. Wang, Y. Wang, *Chem. Soc. Rev.* **2020**, *49*, 6198.

[8] C. Y. Toe, C. Tsounis, J. Zhang, H. Masood, D. Gunawan, J. Scott, R. Amal, *Energy Enivron. Sci.* **2021**, *14*, 1140.

[9] M. F. Kuehnel, E. Reisner, *Angew. Chem., Int. Ed.* **2018**, *57*, 3290, *Angew. Chem.* **2018**, *130*, 3346.

[10] D. I. Kondarides, V. M. Daskalaki, A. Patsoura, X. E. Verykios, *Catal. Lett.* **2008**, *122*, 26.

[11] Q. Xiang, J. Yu, M. Jaroniec, *J. Am. Chem. Soc.* **2012**, *134*, 6575.

[12] T. Uekert, H. Kasap, E. Reisner, *J. Am. Chem. Soc.* **2019**, *141*, 15201.

[13] T. Kawai, T. Sakata, *Nature* **1980**, *286*, 474.

[14] C. M. Pichler, T. Uekert, E. Reisner, *Chem. Commun.* **2020**, *56*, 5743.

[15] X. Chen, S. S. Mao, *Chem. Rev.* **2007**, *107*, 2891.

[16] H. Luo, J. Barrio, N. Sunny, A. Li, L. Steier, N. Shah, I. E. L. Stephens, M.-M. Titirici, *Adv. Energy Mater.* **2021**, DOI:10.1002/aenm.202101180.

[17] J. L. White, M. F. Baruch, J. E. Pander, Y. Hu, I. C. Fortmeyer, J. E. Park, T. Zhang, K. Liao, J. Gu, Y. Yan, T. W. Shaw, E. Abelev, A. B. Bocarsly, *Chem. Rev.* **2015**, *115*, 12888.

[18] A. D. Handoko, K. Li, J. Tang, *Curr. Opin. Chem. Eng.* **2013**, *2*, 200.

[19] R. Francke, B. Schille, M. Roemelt, *Chem. Rev.* **2018**, *118*, 4631.

[20] G. A. Olah, A. Goeppert, G. K. S. Prakash, *Beyond Oil and Gas: The Methanol Economy, 2nd ed.*, Wiley-VCH: Weinheim, Germany, **2011**.

[21] J. Yang, W. Ma, D. Chen, A. Holmen, B. H. Davis, *Appl. Catal. A* **2014**, *470*, 250.

[22] L. Yuan, M.-Y. Qi, Z.-R. Tang, Y.-J. Xu, *Angew. Chem., Int. Ed.* **2021**, DOI:10.1002/anie.202101667.

[23] C. Han, Y.-H. Li, J.-Y. Li, M.-Y. Qi, Z.-R. Tang, Y.-J. Xu, *Angew. Chem., Int. Ed.* **2021**, *60*, 7962.

[24] X. Li, J. Yu, M. Jaroniec, X. Chen, *Chem. Rev.* **2019**, *119*, 3962; *Angew. Chem.* **2021**, *134*, 8041.

[25] H. Gerischer, A. Heller, *J. Electrochem. Soc.* **1992**, *139*, 113.

[26] A. L. Linsebigler, G. Lu, J. T. Yates, *Chem. Rev.* **1995**, *95*, 735.

[27] Y. Ma, X. Wang, Y. Jia, X. Chen, H. Han, C. Li, *Chem. Rev.* **2014**, *114*, 9987.

[28] K. E. Dalle, J. Warnan, J. J. Leung, B. Reuillard, I. S. Karmel, E. Reisner, *Chem. Rev.* **2019**, *119*, 2752.

[29] J. J. Leung, J. Warnan, K. H. Ly, N. Heidary, D. H. Nam, M. F. Kuehnel, E. Reisner, *Nature Catal.* **2019**, *2*, 354.

[30] A. Perazio, G. Lowe, R. Gobetto, J. Bonin, M. Robert, *Coord. Chem. Rev.* **2021**, *443*, 214018.

[31] R. Boissezon, J. Muller, V. Beaugeard, S. Monge, J.-J. Robin, *RSC Adv.* **2014**, *4*, 35690.

[32] C. Enachescu, I. Krivokapic, M. Zerara, J. A. Real, N. Amstutz, A. Hauser, *Inorg. Chim. Acta* **2007**, *360*, 3945.

[33] C. D. Windle, E. Pastor, A. Reynal, A. C. Whitwood, Y. Vaynzof, J. R. Durrant, R. N. Perutz, E. Reisner, *Chem. Eur. J.* **2015**, *21*, 3746.
[34] C. Bozal-Ginesta, C. A. Mesa, A. Eisenschmidt, L. Francàs, R. B. Shankar, D. Antón-García, J. Warnan, J. Willkomm, A. Reynal, E. Reisner, J. R. Durrant, *Chem. Sci.* **2021**, *12*, 946.
[35] Y. Pellegrin, F. Odobel, *C. R. Chim.* **2017**, *20*, 283.
[36] G. Redmond, D. Fitzmaurice, *J. Phys. Chem.* **1993**, *97*, 1426.
[37] J.-S. Lee, D.-I. Won, W.-J. Jung, H.-J. Son, C. Pac, S. O. Kang, *Angew. Chem., Int. Ed.* **2017**, *56*, 976; *56*, 976; *Angew. Chem.* **2017**, *129*, 996.
[38] D.-I. Won, J.-S. Lee, J.-M. Ji, W.-J. Jung, H.-J. Son, C. Pac, S. O. Kang, *J. Am. Chem. Soc.* **2015**, *137*, 13679.
[39] E.-G. Ha, J.-A. Chang, S.-M. Byun, C. Pac, D.-M. Jang, J. Park, S. O. Kang, *Chem. Commun.* **2014**, *50*, 4462.
[40] M. S. Choe, S. Choi, S.-Y. Kim, C. Back, D. Lee, H. S. Lee, C. H. Kim, H.-J. Son, S. O. Kang, *Inorg. Chem.* **2021** DOI:10.1021/acs.inorgchem.1c00615
[41] M. Miller, W. E. Robinson, A. R. Oliveira, N. Heidary, N. Kornienko, J. Warnan, I. A. C. Pereira, E. Reisner, *Angew. Chem., Int. Ed.* **2019**, *58*, 4601; *58*, 4601; *Angew. Chem.* **2019**, *131*, 4649.
[42] T. W. Woolerton, S. Sheard, E. Reisner, E. Pierce, S. W. Ragsdale, F. A. Armstrong, *J. Am. Chem. Soc.* **2010**, *132*, 2132.
[43] R. I. Bickley, T. Gonzalez-Carreno, J. S. Lees, L. Palmisano, R. J. D. Tilley, *J. Solid State Chem.* **1991**, *92*, 178.
[44] D. C. Hurum, A. G. Agrios, K. A. Gray, T. Rajh, M. C. Thurnauer, *J. Phys. Chem. B* **2003**, *107*, 4545.
[45] T. Thiounn, R. C. Smith, *J. Polym. Sci.* **2020**, *58*, 1347.
[46] F. H. Isikgor, C. R. Becer, *Polym. Chem.* **2015**, *6*, 4497.
[47] H. W. Tan, A. R. Abdul Aziz, M. K. Aroua, *Renew. Sustain. Energy Rev.* **2013**, *27*, 118.
[48] I. Abdouli, M. Eternot, F. Dappozze, C. Guillard, N. Essayem, *Catal. Today* **2021**, *367*, 268.
[49] X. Liu, X. Duan, W. Wei, S. Wang, B.-J. Ni, *Green Chem.* **2019**, *21*, 4266.
[50] V. Juturu, J. C. Wu, *Renew. Sustain. Energy Rev.* **2014**, *33*, 188.
[51] C. M. Payne, B. C. Knott, H. B. Mayes, H. Hansson, M. E. Himmel, M. Sandgren, J. Ståhlberg, G. T. Beckham, *Chem. Rev.* **2015**, *115*, 1308.

Entry for the Table of Contents

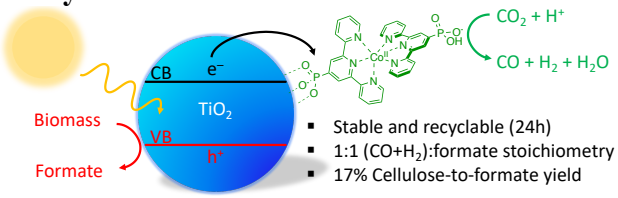

A hybrid photocatalyst consisting of an immobilized phosphonated cobalt bis(terpyridine) catalyst on TiO_2 allows coupling of aqueous CO_2-to-syngas (CO and H_2) photoreduction with the selective photo-oxidation of biomass-derived oxygenates or cellulose to formate. It demonstrates the proof-of-concept of using a single photocatalyst to convert two waste streams in separate half-reactions to produce sustainable chemicals and energy carriers.

Institute and/or researcher Twitter usernames: @ReisnerLab